Numerical Prediction of Pellet Injection Effects on Core Plasma Fueling in the KSTAR Tokamak

Ki Min Kim, Hyunsun Han, Yong-Su Na, and Sang Hee Hong
Department of Nuclear Engineering, Seoul National University, Seoul 151-742, Korea

Abstract

Since pellet injection into tokamak plasmas has been found to be an effective method for fueling and profile modification of core plasmas in tokamak experiments, a hypothetical injection of deutrium pellets into the KSTAR tokamak is numerically simulated in this work to investigate its influences on the fueling and transport of the core plasma depending on pellet parameters. A neutral gas shielding model and a pellet drift displacement model are used to describe the ablation and mass deposition from pellets on core plasma profiles. These models are coupled with a 1.5-dimensional (1.5D) core transport code to calculate the plasma density and temperature profiles responding to pellets injected into the target plasma. The simulation results indicate that a HFS (high field side) injection achieves more effective fueling due to a deeper pellet penetration into the core plasma, compared with a LFS (low field side) injection. The plasma density is found to increase during sequential pellet injections from both HFS and LFS, but the HFS case shows better fueling performance owing to a drift of the pellet ablatant in the major radius direction resulting in the deeper pellet penetration. Increasing the size and injection velocity of the pellet contributes to enhance the fueling efficiency. However, raising the power of neutral beam injection heating reduces the fueling efficiency because the pellet mass deposition is shifted toward the edge region in high temperature plasmas. It is concluded that the pellet size and injection direction among pellet and plasma parameters have the most dominant effects on fueling performance while the pellet velocity and heating power have relatively small influences on fueling.

Keywords: Pellet injection, Fueling, Tokamak Transport, KSTAR

1. Introduction

Pellet injection is regarded as one of useful candidates for plasma core fueling and plasma profile control, which have been demonstrated in various tokamak experiments to provide efficient fueling, induced changes in plasma transport, edge-localized mode (ELM) triggering, and so on. Both theoretical and experimental studies on the pellet injection have been widely performed over the past three decades; however, the physics of pellet fuelling and subsequent plasma behaviors are not fully understood yet [1, 2].

Early experiments performed on ASDEX Upgrade found that the high field side (HFS) injection of hydrogenic pellets could dramatically improve the pellet fueling efficiency compared to the low field side (LFS)

injection [3]. Later pellet experiments on DIII-D also have reported the similar results that the injection from HFS achieved a deeper penetration of pellet fuel so that the fueling efficiency was enhanced [4]. Recently the high speed pellet injections from HFS and LFS are considered as promising methods for deep core fueling in present-day tokamaks and even in ITER [5, 6]. Since the KSTAR superconducting tokamak, newly built at NFRI (National Fusion Research Institute) in Korea, aims to achieve a high density operation, it urgently needs not only the prediction of pellet fueling characteristics but also the development of effective pellet injection scenarios [7].

Once a frozen pellet enters the target plasma, pellet particles begin to be immediately ablated from the pellet surface and ionized to ions and electrons during its penetration through a hot plasma environment. The ion and electron particles are then deposited on the target plasma after the drift motions caused by the magnetic field gradients in tokamaks. The deposited particles diffuse outward in the major radius direction (or inward and outward in the poloidal radius direction, respectively) in HFS and LFS injections, and sometimes are released to the outside of the core plasma by ELM crashes [1, 2]. Such particle transports can govern the entire plasma transport and overall tokamak performances. It is important to predict the plasma behaviors related to the pellet fueling for achieving high density tokamak plasmas and designing an appropriate injection system in KSTAR. However, transport analyses which simultaneously describe the plasma transport along with the injected pellet transport have been scarcely reported, and thus the transport phenomena in pellet injected plasmas observed in the experiments have not been sufficiently interpreted so far. Therefore, a transport modeling study including pellet injection effects is essentially needed for the high density operations in KSTAR and ITER.

In this paper, the pellet fuel deposition and particle transport are numerically simulated for the KSTAR operation scenarios by using a 1.5D core transport code combined with the pellet injection models. Numerical models for core plasma transport and pellet injection applied in this work are described in section 2. Simulation results of pellet fueling are presented in section 3 for various operation parameters such as injection direction, pellet size, pellet velocity, and neutral beam injection (NBI) heating power. In section 4, the effects of the operation parameters on fueling and transport characteristics are discussed, and the engineering and physical requirements for an efficient pellet fueling in KSTAR tokamak are suggested. Section 5 summarizes the present simulation work in this paper.

2. Theoretical formulation and numerical modeling of pellet-injected plasma transport

A 1.5D transport code [8] is upgraded to calculate the heat and particle transport in the tokamak core region before and after pellet injection. The plasma transport in the core region is described by the continuity equation of electron density, the momentum equations of electron and ion, and the current diffusion equation, which calculate the time evolution of plasma density and temperature in response to the pellet injection self-consistently. Especially, the evolution of the electron density n_e is calculated by the continuity equation:

$$\frac{\partial n_e}{\partial t} + \nabla \cdot \vec{\Gamma}_e = S_e \quad , \qquad (1)$$

where S_e is the particle source, and $\vec{\Gamma}_e$ is the electron particle flux due to diffusion and inward pinch [9, 10], which is expressed in this modeling as

$$\vec{\Gamma}_e = -D\nabla n_e + n_e \vec{v}_{in} , \qquad (2)$$

where D is the particle diffusion coefficient and $\vec{v}_{in}$ is the neoclassical inward pinch velocity [11, 12]. The pinch term represents the inward particle motions to the core axis, while the diffusion term represents the outward particle motions toward the edge region. The thermal diffusivities χ of electron and ion are calculated as the sum of neoclassical and anomalous transport coefficients which are expressed as

$$\chi_e = \chi_e^{NEO} + \chi_e^{ITG/TEM} + \chi_e^{RB} + \chi_e^{KB} + \chi_e^{ETG} , \qquad (3)$$

$$\chi_i = \chi_i^{NEO} + \chi_i^{ITG/TEM} + \chi_i^{RB} + \chi_i^{KB} . \qquad (4)$$

It has been reported that the particle diffusivity is related with the thermal diffusivities of electron and ion, where the particle diffusion coefficient can be estimated by a relation of $D \sim 0.3\chi_{eff}$ where $\chi_{eff} = (\chi_e + \chi_i)/2$ [13]. In this numerical work, χ_{eff} is assumed as $(2\chi_e + \chi_i)/3$ giving an impact on the electron thermal transport so that the particle diffusivity D is calculated by an equation expressed as

$$D = 0.1 \times (2\chi_e + \chi_i) . \qquad (5)$$

In the above expressions for both electron and ion, a theory-based multi-mode model (MMM) [14] has been employed for calculating the anomalous contributions caused by the ion temperature gradient (ITG) mode, trapped electron mode (TEM), resistive ballooning (RB) mode, and kinetic ballooning (KB) mode. Particularly, an additional contribution from the electron temperature gradient (ETG) mode given by the Horton model [15] is added to the electron thermal diffusivity calculations. The typical profile of particle diffusion coefficient calculated from the transport models is presented in Fig. 1.

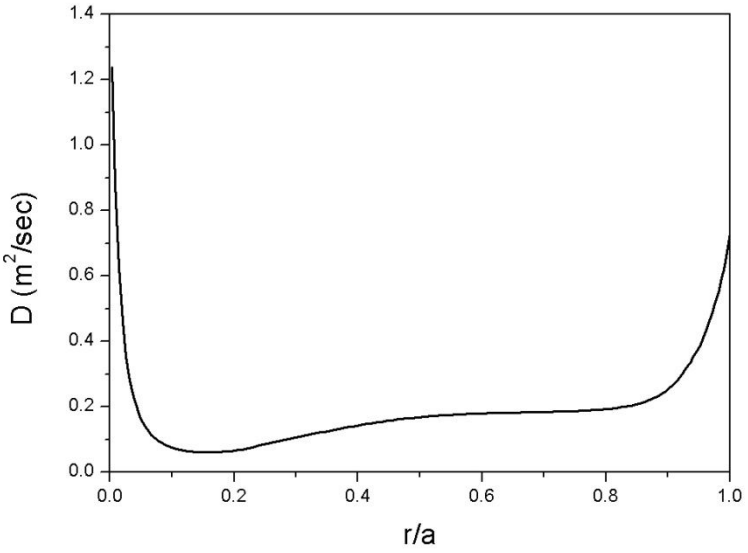

Fig. 1. A typical profile of particle diffusion coefficient estimated from this numerical work. Calculation conditions are adopted from the KSTAR parameters given in Table 1 when 4 MW of NBI power is applied.

H-mode plasmas are considered as target plasmas for pellet fueling by introducing an L-H transition model and an edge turbulence suppression model. The H-mode transition from an L-mode is assumed to occur when the plasma power across the separatrix exceeds an H-mode threshold power scaled by the ITER database [16]. After an H-mode transition, the turbulence suppression functions composed of magnetic and rotational shears [17] are switched on so that an H-mode pedestal build up. Every pellet is injected after the H-mode transition. The machine and plasma parameters of the KSTAR tokamak used in the transport calculations are listed in Table 1.

Table 1. Plasma and operation parameters of KSTAR used in the simulation

KSTAR Parameters	
Major radius	1.8 m
Minor radius	0.5 m
Triangularity at separatrix	0.6
Elongation at separatrix	2.0
Plasma current	2.0 MA
Toroidal magnetic field	3.5 T
Plasma species	Deuterium
Auxiliary heating method, power	NBI, 4~8 MW

A neutral gas shielding (NGS) model [18] has been applied to calculate pellet ablation rates during the pellet penetration through the target tokamak plasmas. The NGS model is based on the formation of a symmetric and spherically expanding neutral cloud of the pellet material with the help of the energy transport from background plasmas to the pellet. It assumes monoenergetic electron beams which impact onto the surface of neutral cloud surrounding the injected pellet. Although the NGS model is a simple approximation, it has been well known to show reasonable agreements with various tokamak experiments. According to the NGS model, the pellet ablation rate, the total number of ablated particles per second $\dot{N}$, is expressed as the following power function:

$$\dot{N} = 1.12 \times 10^{16} n_e^{0.333} T_e^{1.64} r_p^{1.333} M_i^{-0.333} \tag{6}$$

where T_e and n_e are the electron temperature in eV and density in cm^{-3}, respectively. r_p is the pellet radius in cm, and M_i is the atomic mass of pellet material, e.g., $M_i = 2$ for deuterium in this modeling. The shape of the injected pellets is assumed as sphere, and the radii of three kinds of pellets considered in the simulation are 1.0 mm, 1.2 mm and 1.55 mm, respectively. These spherical pellets are equivalent to the cylindrical pellets of equal diameter and length of 1.8 mm, 2.1 mm, and 2.8 mm, respectively. The number of atoms contained in each pellet is estimated to be 1.3 x 10^{20}, 2.2 x 10^{20} and 4.6 x 10^{20}, respectively.

Once a pellet injected into the hot plasma ablates along its passage through the target plasma, the ablated particles are immediately ionized as fuel plasmas that experience drift motions in the direction of major radius, caused by the variation of the magnetic field in tokamaks [19, 20]. To include this drift effect, a newly reported scaling model of pellet drift displacement, which is based on the grad-B induced pellet drift [21, 22], has been taken into account in the modeling as follows:

$$\Delta_{drift} = c_1 v_p^{c_2} r_p^{c_3} n_{e0}^{c_4} T_{e0}^{c_5} \left(\left| |\theta| - c_6 \right| + c_7 \right)^{c_8} \left(1.0 - \Lambda\right)^{c_9} a_0^{c_{10}} R_0^{c_{11}} B_0^{c_{12}} \kappa^{c_{13}}, \tag{7}$$

where T_{e0} and n_{e0} are the electron temperature and density at the plasma core axis. The suggested drift model scales the drift displacement Δ_{drift} with pellet velocity v_p, injection angle θ, minor radius a_0, major radius R_0, toroidal magnetic field B_0, and plasma elongation κ. Here, the impact parameter of the pellet trajectory Λ is assumed as 0 in the drift calculation. Coefficient and power parameters c_s (s = 1, 2, …, 13) in Eq. (7) are described in Reference 18. For every simulation condition, the pellet injections from HFS midplane and LFS midplane are taken into account as depicted in Fig. 2.

The initial plasma density before pellet injection is assumed to have a parabolic profile with 6.0 x 10^{19} m^{-3} at the core axis and 2.0 x 10^{19} m^{-3} at the separatrix, as shown in Fig. 3 (a). The time traces of ohmic plasma current and NBI heating power are presented in Fig. 3 (b), respectively. The plasma current ramps up to 2 MA during initial 2 seconds of an ohmic discharge, while the NBI heating is applied at 2.5 second in the flat-top phase. A

reference NBI power is set as 4 MW and the power is raised to 8 MW to estimate the effects of heating power on pellet fueling.

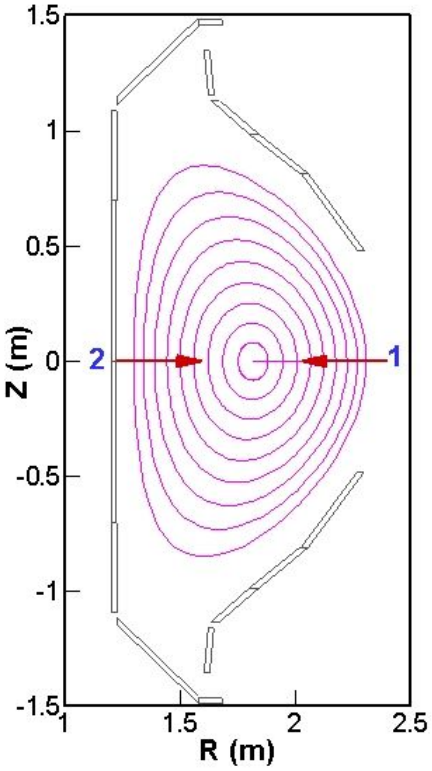

Fig. 2. Pellet injection locations on the KSTAR Tokamak mapped on a poloidal cross section: LFS midplane (1) and HFS midplane (2)

(a)

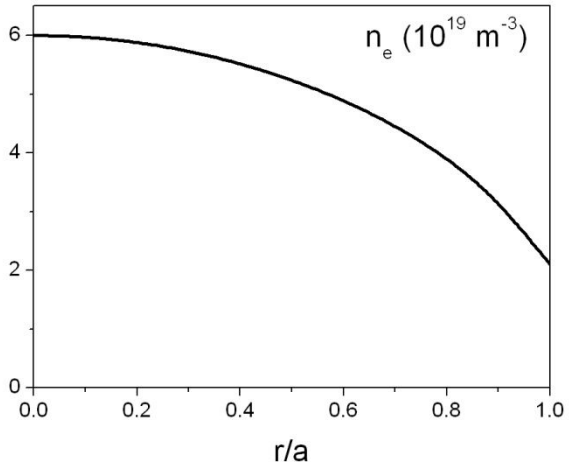

(b)

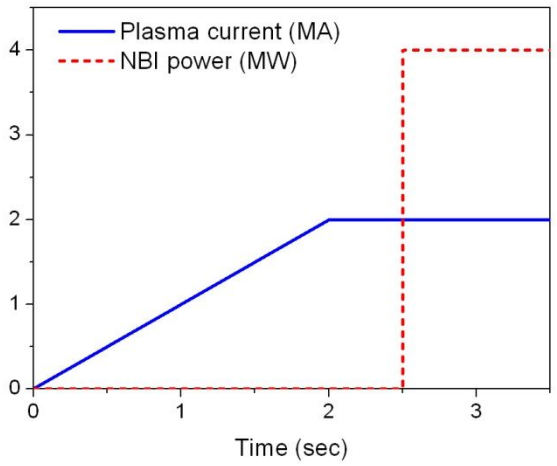

Fig. 3. (a) Initial electron density profile before pellet injection, and (b) time traces of ohmic plasma current ramp-up and NBI heating power.

3. Results of Numerical Simulation

The fueling characteristics are compared according to various operation parameters of both the injected pellet and the target plasmas. Evolutions of plasma densities are represented by line-integrated and volume-averaged electron densities, where the line-integrated density evolutions are calculated along the line on the midplane passing through the magnetic axis.

3. 1. Effects of pellet parameters on fueling

Firstly, the direction effects of pellet injection are compared between HFS and LFS injections with the same values of the pellet parameters under the same target plasma condition. Fig. 4 shows the time evolutions of line-integrated and volume-averaged electron densities during the periodic injections of deuterium pellets of 1.55 mm in radius at 200 m/s of injection velocity from HFS and LFS midplane, respectively. In all these cases, the target plasma is heated by NBI with a fixed power of 4 MW.

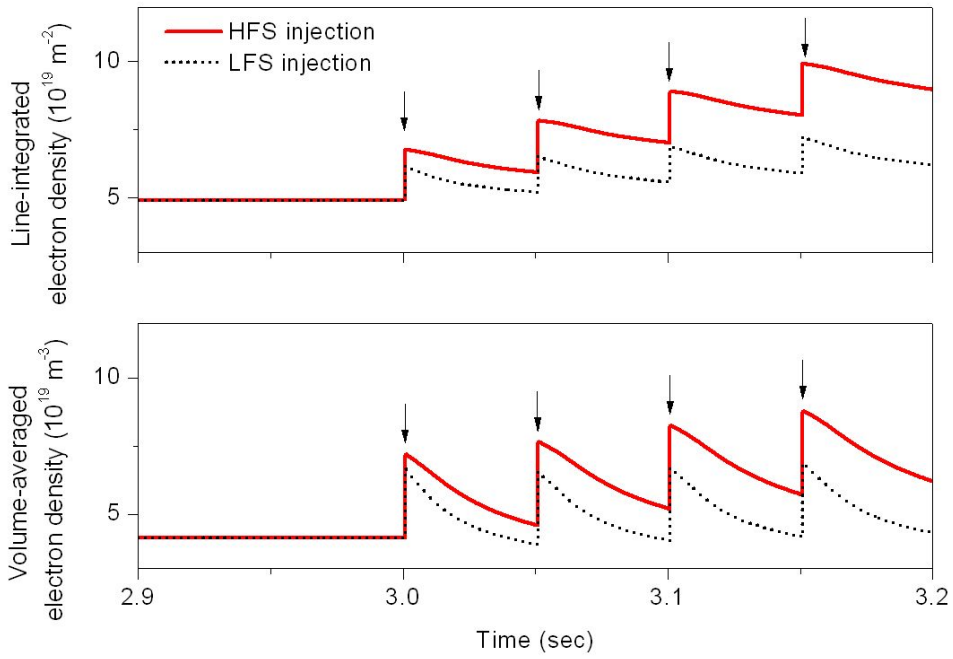

Fig. 4. Time evolution of line-integrated (top) and volume-averaged (bottom) electron densities during sequential pellet injections from HFS and LFS, respectively (r_p = 1.55 mm, v_p = 200 m/s, and P_{NBI} = 4MW). Arrow indicates the moment of each pellet injection.

It is seen from Fig. 4 that both line-integrated and volume-averaged densities abruptly increase right after each pellet injection. After each pellet injection, the ionized particles diffuse and eventually drift inward or outward from their ablated positions depending on the injection direction, so the plasma particles go through density relaxation until the next pellet injection. The line-integrated densities are estimated to be increased by up

to 37 % and 25 %, respectively, after each HFS and LFS injection. This indicates that the injection from HFS is more efficient for fueling than the one from LFS, which can be explained by deeper pellet penetration in the HFS injection [3, 4, 6]. The difference in the depth of pellet mass deposition between HFS and LFS is appeared more apparently in Fig. 5, which show the radial profiles of the electron density increment due to pellet ablation and mass deposition in HFS and LFS injections into a D-shaped tokamak plasma in H-mode with a fixed electron temperature profile, for simplicity.

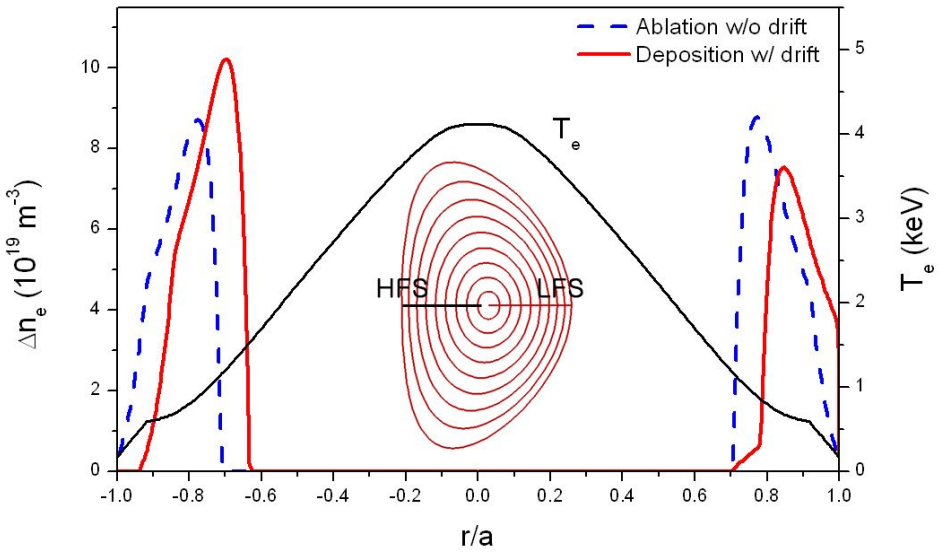

Fig. 5. Radial profiles of pellet ablation and deposition according to the methods of injection into the D-shaped background plasma of minor radius *a* with a fixed temperature profile (r_p = 1.55 mm, v_p = 200 m/s, and P_{NBI} = 4MW). Injection from HFS midplane (left) predicts a deep depth of pellet mass depostion, while one from LFS midplane (right) predicts a shallow edge deposition. Solid lines indicate the deposition profiles of injected pellets, and dashed lines represent the ablation profiles without considering pellet drift motions.

The Fig. 5 indicates that the pellet injected from HFS penetrates into the deeper plasma region up to r/a ~ 0.6 while that from LFS moves back to the injected direction and cannot reach beyond r/a ~ 0.8 toward the plasma core. The pellet injected from LFS hardly reaches the central region, and thus provides relatively shallow depth of pellet mass deposition and poor fueling. These modeling results reasonably agree with the previous experimental results of other tokamaks [3, 4, 6].

Fig. 6 and 7 exhibit the effects of pellet size on the plasma density evolution and on the pellet mass deposition, respectively. The pellet size is varied with its radius r_p while the NBI heating power and the pellet injection velocity are fixed at 4 MW and 200 m/s, respectively. It is observed in Fig. 6 that the large pellet achieves better fueling in both HFS and LFS injections compared to the small pellet. This is because the life time of a large pellet for its complete ablation is much longer than that of a small pellet. Fig. 6 also reveals that the injection of small pellet from LFS could not provide sufficient fueling deeply into the central plasma region due to the lack of containing particles on the way from the edge to core plasmas. Instead, the small pellet supplies the ablated

particles almost in the edge region, and, to make matters worse, most of them drift back to the injection direction and are eventually deposited in the peripheral region of the tokamak plasmas.

Such pellet injection behavior can be reaffirmed in Fig. 7, which shows for both LFS and HFS that a large pellet delivers much more fuel particles into the central region than a small pellet. The depth of pellet mass deposition reaches up to r/a ~ 0.6 from the separatrix in HFS injection while it stops shorter at r/a ~ 0.8 in LFS injection. These results support the previous statement concerning the longer lifetime of the large pellet injected from HFS.

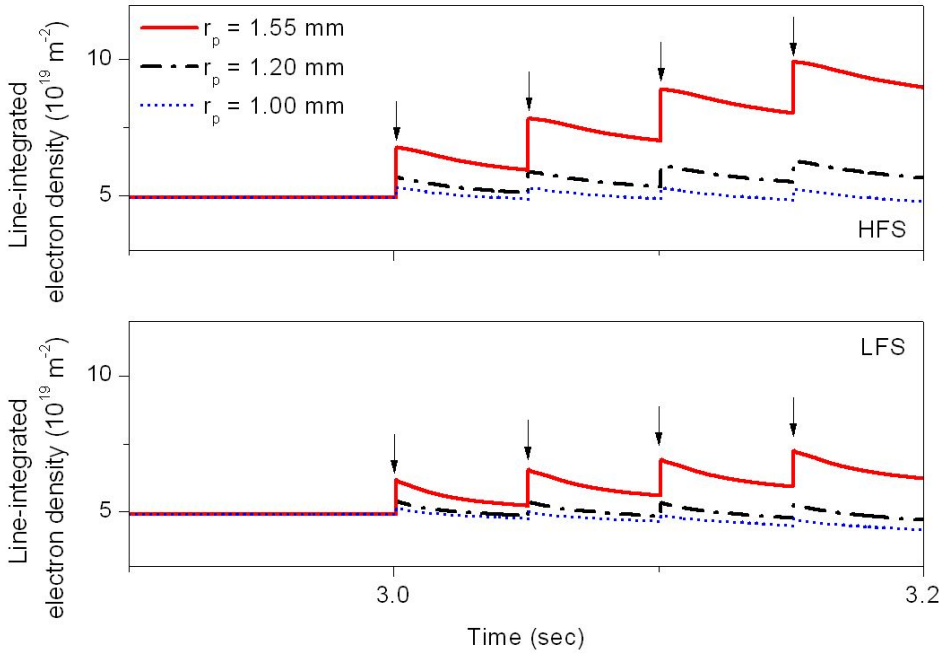

Fig. 6. Time evolution of line-integrated electron density during sequential pellet injections from HFS (top) and LFS (bottom) with three different pellet sizes (v_p = 200 m/s and P_{NBI} = 4MW).

(a)

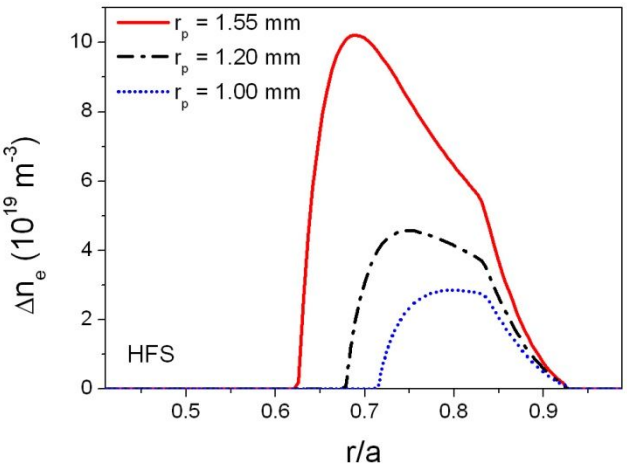

(b)

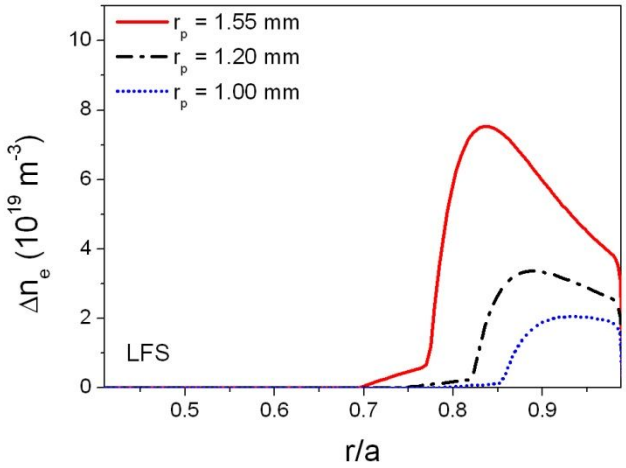

Fig. 7. Comparison of the deposition profiles of pellet mass among three different pellet sizes: (a) HFS injection and (b) LFS injection (v_p = 200 m/s and P_{NBI} = 4MW).

The fueling influences of the pellet injection velocity can be found in Fig. 8, for which the NBI power and pellet radius are fixed at 4 MW and 1.55 mm, respectively, in the simulation. As similar to the effects of the large pellet size, the high injection velocity contributes to better fueling performance in both HFS and LFS injections. Higher the velocity becomes, longer the pellet survives after the injection during its passage through the target plasma from the edge to the deeper penetration region. In this respect, even the LFS injection is expected to improve its fueling efficiency by a high velocity injection. Comparison of the mass deposition profiles appeared in Fig. 9 illustrates that as the injection velocity increases, the depth of pellet mass deposition becomes deeper toward the core plasma in both LFS and HFS injections. This can be explained by the same way of the pellet size case. At 300 and 200 m/s of the injection velocity, the pellet reaches deep up to r/a ~ 0.55 and 0.6, respectively, in the HFS injection, while shallow near r/a ~ 0.7 and 0.77 in the LFS injections.

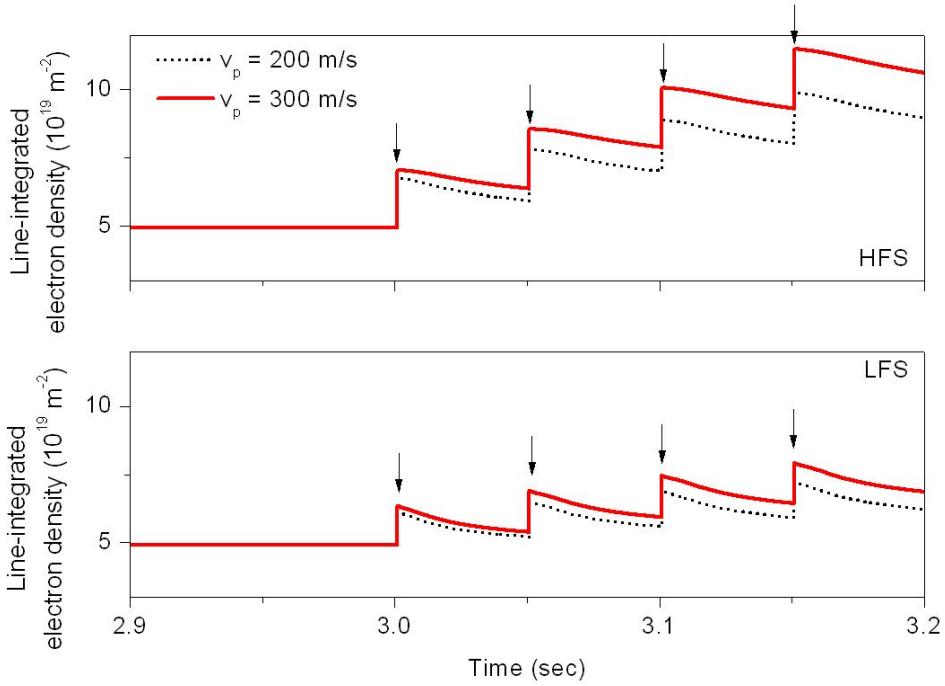

Fig. 8. Time evolution of line-integrated electron density during sequential pellet injections from HFS (top) and LFS (bottom) with two different injection velocities (r_p = 1.55 mm and P_{NBI} = 4MW).

(a)

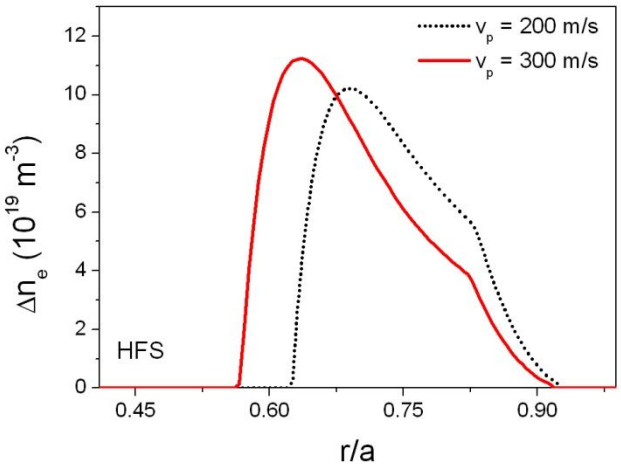

(b)

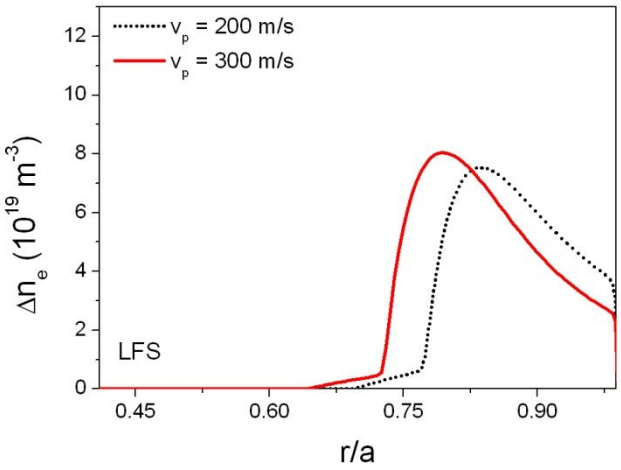

Fig. 9. Comparison of the deposition profiles of pellet mass between two different injection velocities: (a) HFS injection and (b) LFS injection (r_p = 1.55 mm and P_{NBI} = 4MW).

3. 2. Effects of NBI heating power on fueling

Auxiliary heating of tokamak plasmas, such as NBI heating, also has influence on the pellet fueling properties by changing the target plasma transport. Hot plasmas with high temperature as well as high density in H-mode are essentially required for achieving both ignition and confinement conditions to practically generate high fusion powers in tokamaks. Even though NBI heating is one of the most promising methods for achieving high temperature plasmas, it has been reported that the efficiency of pellet fueling for raising plasma density decreases with increasing NBI heating power [3, 23]. Since the pellet injection is the most useful method for core plasma fueling, the high-power NBI heating to obtain high temperature plasmas may cause the efficient

pellet fueling to deteriorate. Although the NBI itself provides particle fuel to plasmas, its fueling effects are known to be negligible compared to pellet fueling.

In order to verify this undesirable NBI effect, the pellet fueling has been simulated by changing NBI power with the fixed pellet parameters of 1.55 mm pellet radius and 200 m/s injection velocity. When the NBI powers of 4, 6, 8 MW are applied, the electron temperatures are estimated as 4.2, 4.5, 4.8 keV at the core axis, and 0.59, 0.64, 0.68 keV at the pedestal, respectively. As seen in Fig.10, it is confirmed that elevating the NBI heating power reduces the fueling effect in both HFS and LFS injections as experimental observations [3, 23]. The target plasma of higher temperatures increased by a high NBI heating power enhances blocking the penetration of injected pellets since the increased plasma temperature accelerates the ablation process. The NGS model indicates that the pellet ablation rate is proportional to the background plasma temperature and density, and more strongly depends on temperature [17, 24]. The reduced depths of pellet mass depositions by increasing the NBI powers are more clearly seen in Fig. 11. The pellet mass deposition profiles appear to be shifted toward the edge region of the target plasma as the NBI power increases, and thus the pellet fueling efficiency is worsened. This negative effect of NBI power is not accounted to dominantly reduce the pellet fueling efficiency, but it should not be ignored. Therefore, an additional parameter of NBI heating power to the previously considered pellet parameters should be taken into account for optimizing the pellet injection scenarios under the high power heating.

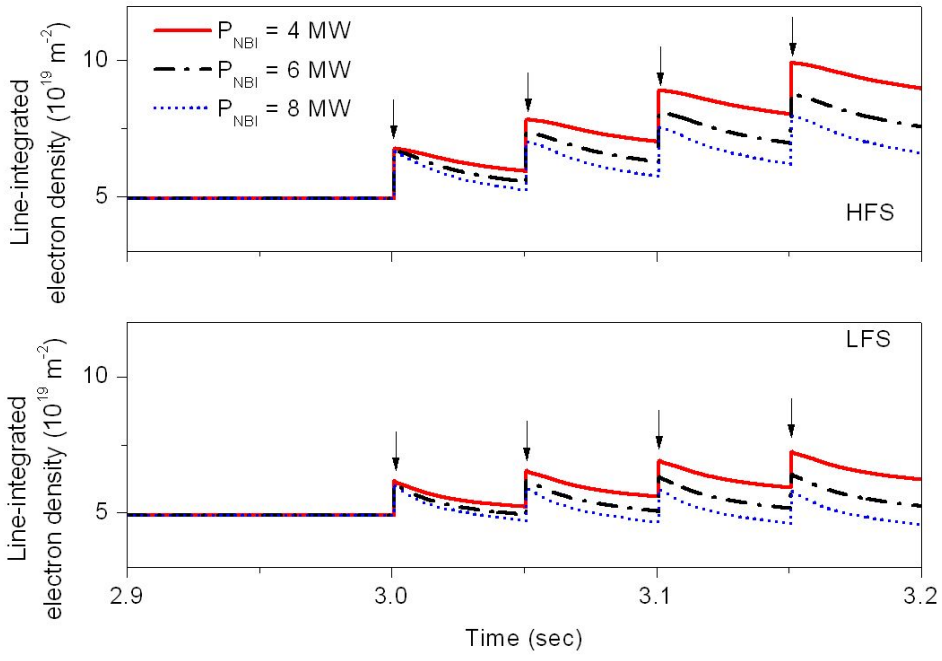

Fig. 10. Time evolution of line-integrated electron density during sequential pellet injections from HFS (top) and LFS (bottom) into the tokamak plasmas heated by NBI with three different powers (r_p = 1.55 mm and v_p = 200 m/s).

(a)

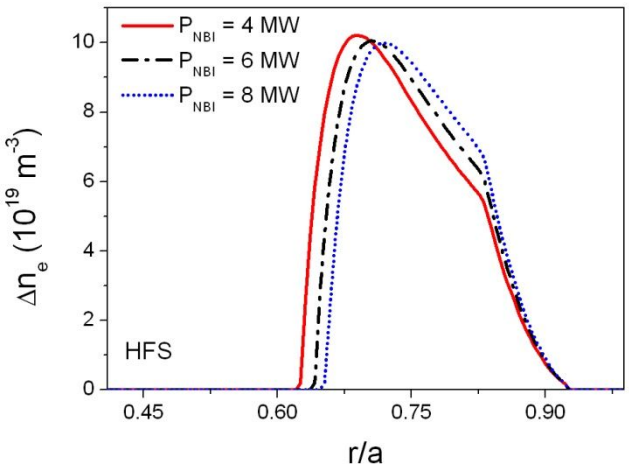

(b)

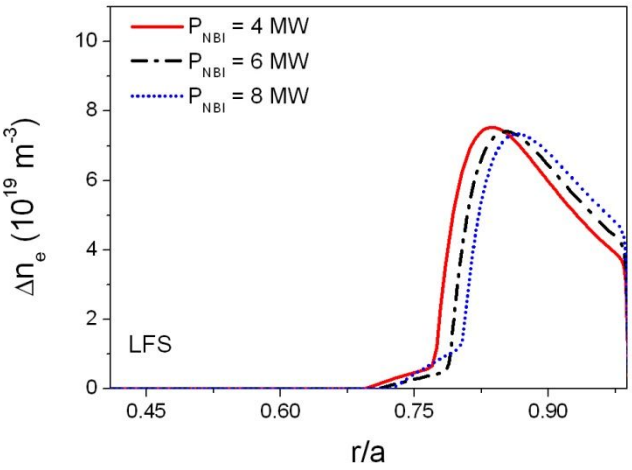

Fig. 11. Comparison of the deposition profiles of pellet mass among three different NBI heating powers: (a) HFS injection and (b) LFS injection (r_p = 1.55 mm and v_p = 200 m/s).

4. Discussion

From the predictions from the present numerical simulation, the dominant factors for the pellet fueling performance can be determined. The simulation results of plasma density enhancements by pellet injection fueling are summarized in Fig. 12. By calculating the line-integrated densities before and after pellet injection,

the plasma density enhancements have been estimated for the pellet and NBI parameters described in the previous sections. In Fig. 12, the 1.55 mm pellet shows around two and a half times higher density enhancement than the 1.2 mm pellet for both the HFS and LFS injections. On the other hand, the density enhancement by the HFS injection is about one and a half times higher than that by the LFS injection, and the 300 m/s injection improves only about 15 % higher than the 200 m/s injection from both HFS and LFS. Even comparing the density enhancement of higher speed injection (300 m/s) from LFS with lower speed injection (200 m/s) from HFS, the HFS injection achieves a better fueling performance. The effect of the NBI heating power turns out to be smallest among all parameters by observing the very slowly decreasing slopes of the density enhancements with increasing the NBI power. In view of these numerical results, the pellet size has the most dominant influence on plasma density enhancement in pellet injection fueling. Therefore, the optimization of the pellet size among all pellet and plasma parameters should be considered as the most important factor in designing a pellet injection system in future devices.

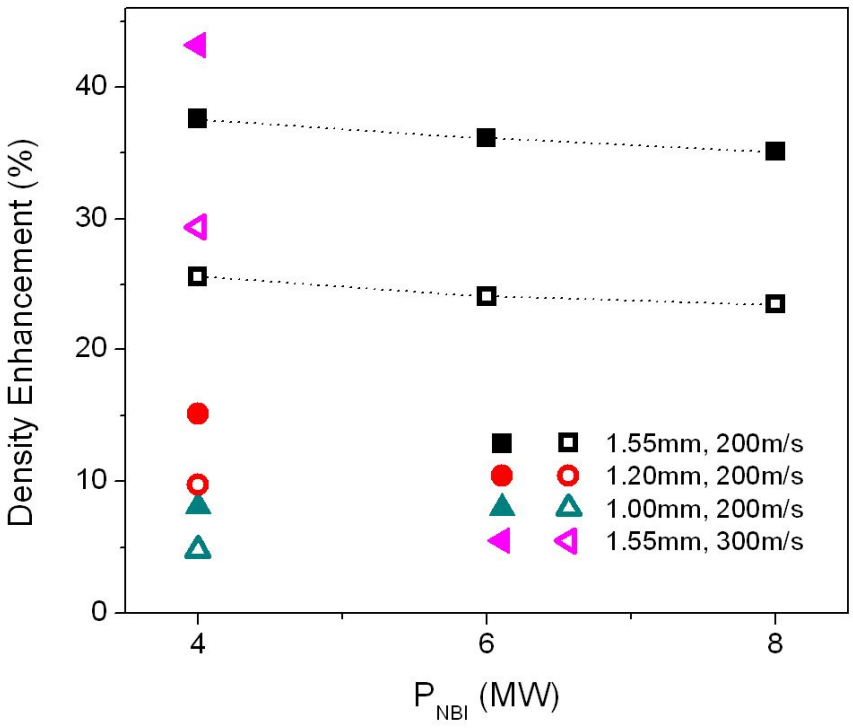

Fig. 12. Plasma density enhancement by HFS (full marks) and LFS (empty marks) injections with different pellet parameters (radius r_p and injection velocity v_p) and NBI heating conditions (P_{NBI}).

The numerical simulation also predicts for KSTAR that the pellet radius larger than r_p = 1.2 mm is required to achieve at least 10 % increment in the electron density by an LFS injection of a single pellet. The required pellet

size becomes to be smaller in an HFS or high velocity injection. It is also predicted that the injection velocity should be higher than 200 m/s to obtain at least 5 - 10 % higher fueling effects in due consideration of the poor fueling of the small pellet injection from LFS. These requirements can be changed according to the plasma conditions and other parameter such as pellet size, but they could be minimal limits.

On the other hand, the operation conditions of pellet fueling should be carefully controlled in case of the large size pellet injection from HFS. The excessive fueling over 30 - 40 % in plasma density enhancements may unexpectedly perturb the target plasmas to cause improper cooling of core plasmas and confinement degradation. The large machines, such as ITER and DEMO, need larger pellets and higher injection velocities than the present-day tokamaks due to enlarged huge plasma volumes. It should be noted that as the pellet size and velocity are larger and higher, respectively, the plasma responses to the pellet fueling can be much stronger. Since even small plasma perturbations in large machines can be disadvantageous to the operations [5], further studies need to be carried out for ITER and DEMO in the near future.

On the contrary, the shallow pellet fueling by small size or low injection velocity might be useful for ELM control. In present-day tokamaks and ITER, the artificial ELM triggering induced by pellet injection has been proposed and being tested in many tokamaks as a control method of ELMs [6, 25, 26]. This, so-called, ELM pacing is promising because the pellet-triggered artificial ELMs have been observed to release lower energy from the core and reduce the divertor heat load, compared with spontaneous ELMs. ELM pacing should be carefully performed with the smallest impact on plasma transport to suppress the core plasma perturbations induced by pellet injection because the stored plasma energy can be affected by pellets used for ELM pacing. The plasma response to pellet injection is basically adiabatic. The plasma pressure profile does not change after pellet injection in spite of the increased density by fueling due to the temperature losses consumed for ionization of the pellet. It was, however, found from this simulation for LFS injection that the particle losses caused by the outward drift make a slight reduction in the plasma stored energy. In case of HFS injection, the stored energy is almost conserved owing to little particle losses when particle losses caused by pellet induced ELM or ELM like activities are not taken into account. If an ELM triggering by pellet injection is considered in the modeling, the stored energy and total particle content will be slightly reduced by the enhanced energy and particle transport of the ELM in both HFS and LFS injections. As a depth of pellet mass deposition is deeper, the reduced amount of stored energy can be larger. In this sense, the pellet injection with the parameters leading to poor fueling would be more useful for ELM pacing. A shallow pellet injection needs to be considered for the design of the KSTAR pellet injection system, and the effects of pellet induced ELMs should be included in the modeling in the future. Unfortunately fueling and ELM pacing by pellets are strongly coupled to make the physics of pellet injection much more complex, so further theoretical and experimental studies are still required.

It is also worth discussing the effects of spontaneous ELMs in H-mode plasmas. If a pellet is injected during the activated phase of spontaneous ELM for less than 1 ms, the effect of ELM-enhanced transport on pellet fueling is unknown. The ELM effects on pellets in this case are beyond a scope of this paper. Nevertheless, we expect that the pellet will behave much complicatedly in ELMy H-mode plasmas. The collapsed edge pedestal by ELM will help a deeper pellet penetration when a pellet is injected during a recovery phase before an ELM

onset. However, ELM particle losses will worsen the overall fueling performance by releasing the fuel particles out of the plasma.

5. Conclusion

In this numerical work, the pellet ablation and drift models are coupled to a core plasma transport code to predict the pellet injection and fueling properties in KSTAR. The HFS injection predicts the deeper penetration of pellet fuels into the target core plasma than the LFS one due to the radial drift motion of an ablated pellet plasma cloud in the major radius direction. The pellet injections with increasing pellet size and injection velocity are expected to contribute to better efficiency of fueling. It is, however, predicted that the small pellet injection from LFS will be difficult to supply sufficient pellet fuels to the core plasmas. Fueling efficiency is even worse in case of the pellet injection with low velocity into high temperature plasmas. The large pellet and high injection velocity are indispensable to achieve sufficient fueling in the LFS pellet injection. Even in the HFS injection, high velocity injection of large pellets is required for better core fueling, especially in large tokamak machines. It is found that the pellet size and injection direction among pellet and plasma parameters have the most decisive effects on fueling performance while the pellet injection velocity has a relatively small influence on fueling. On the other hand, the effects of NBI heating on plasma density enhancement in pellet injections are barely appreciable with increasing heating power, compared to the effects of other pellet parameters. The correlations among NBI heating, target plasma properties, and pellet parameters are not clearly resolved yet, for they are complicatedly linked to one another. Nevertheless, sufficiently high fueling efficiencies will be obtainable with large pellets injected with high velocity from HFS, once a possible excessive fueling is avoided not to perturb the target plasma.

There still exist many challenges to overcome in pellet physics and engineering: optimization of pellet operation, investigation on ELM pacing, extrapolation to ITER, and so on. The transport simulations based on the integrated models of plasma transport and pellet injection in this study can be extended to resolve these challenges. The physical analysis and parameters obtained in this numerical work will be directly applicable to the design of a KSTAR pellet injection system and the scenario development of high density operation with pellet injection. Furthermore, the numerical models developed in this work can be used for a transport analysis of pellet injection in the KSTAR experiments and for the prediction of ELM pacing throughout an extension to physics of ELM and ELM triggering by pellet injection.

Acknowledgements

This work was supported by the Korea Science and Engineering Foundation (KOSEF) grant (No. R11-2008-072-02003-0) funded from the Ministry of Education, Science and Technology (MEST) in Korea.

References

[1] B. Pégourié, Plasma Phys. Control. Fusion 49 (2007) R87

[2] S. L. Milora, W. A. Houlberg, L. L. Lengyel, V. Mertens, Nucl. Fusion 35 (1995) 657

[3] P. T. Lang, K. Büchl, M. Kaufmann, R. S. Lang, V. Mertens, H. W. Müller, J. Neuhauser, ASDEX Upgrade, NI Teams, Phys. Rev. Lett. 79 (1997) 1487

[4] L. R. Baylor, T. C. Jernigan, S. K. Combs, W. A. Houlberg, M. Murakami, P. Gohil, K. H. Burrell, C. M. Greenfield, R. J. Groebner, C. -L. Hsieh, R. J. La Haye, P. B. Parks, G. M. Staebler, The DIII-D Team, G. L. Schmidt, D. R. Ernst, E. J. Synakowski, M. Porkolab, Phys. Plasmas 7 (2000) 1878

[5] L. R. Baylor, P. B. Parks, T. C. Jernigan, J. B. Caughman, S. K. Combs, C. R. Foust, W. A. Houlberg, S. Maruyama, D. A. Rasmussen, Nucl. Fusion 47 (2007) 443

[6] L. R. Baylor, T. C. Jernigan, P. B. Parks, G. Antar, N. H. Brooks, S. K. Combs, D. T. Fehling, C. R. Foust, W. A. Houlberg, G. L. Schmidt, Nucl. Fusion 47 (2007) 1598

[7] M. Kwon, Y. S. Na, J. H. Han, S. Cho, H. Lee, I. K. Yu, B. G. Hong, Y. H. Kim, S. R. Park, H. T. Seo, Fusion Eng. Des. 83 (2008) 883

[8] K. M. Kim, H. Han, E. S. Yoon, J. M. Park, S. H. Hong, J. Korean Phys. Soc. 49 (2006) S215

[9] TFR Group, Nucl. Fusion 27 (1987) 1975

[10] G. Kamelander, G. Weimann, L. Garzotti, X. Litaudon, D. Moreau, B. Pégourié, Fusion Sci. Technol. 46 (2004) 558

[11] A. A. Ware, Phys. Rev. Lett. 25 (1970) 15

[12] F. L. Hinton, R. D. Hazeltine, Rev. Mod. Phys. 48 (1978) 239

[13] J. Stober et al., Nucl. Fusion 41 (2001) 1535

[14] G. Bateman, A. H. Kritz, J. E. Kinsey, A. J. Redd, J. Weiland, Phys. Plasmas 5 (1998) 1793

[15] W. Horton, P. Zhu, G. T. Hoang, T. Aniel, M. Ottaviani, X. Garbet, Phys. Plasmas 7 (2000) 1494

[16] Y. Shimomura, Y. Murakami, A. R. Polevoi, P. Barabaschi, V. Mukhovatov, M. Shimada, Plasma Phys. Control. Fusion 43 (2001) A385

[17] A. Y. Pankin, I. Voitsekhovitch, G. Bateman, A. Dnestrovski, G. Janeschitz, M. Murakami, T. Osborne, A. H. Kritz, T. Onjun, G. W. Pacher, H. D. Pacher, Plasma Phys. Control. Fusion 47 (2005) 483

[18] P. B. Parks, R. J. Turnbull, Phys. Fluids 21 (1978) 1735

[19] P. B. Parks, W. D. Sessions, L. R. Baylor, Phys. Plasmas 7 (2000) 1968

[20] H. R. Strauss, W. Park, Phys. Plasmas 5 (1998) 2676

[21] F. Köchl, D. Frigione, L. Garzotti, G. Kamelander, H. Nehme, B. Pégourié, JET EFDA contributors, Proc. 35th EPS Conf. Plasma Phys. 32D, P-4.099, 9-13 June 2008, Hersonissos, Greece

[22] B. Pégourié, V. Waller, H. Nehme1, L. Garzotti, A. Géraud, Nucl. Fusion 47 (2007) 44

[23] P. T. Lang, H. Zohm, K. Buchl, J.C. Fuchs, O. Gehre, O. Gruber, V. Mertens, H. W. Muller, J. Neuhauser, ASDEX Ugrade Team, NBI Team, Nucl. Fusion 36 (1996) 1531

[24] L. R. Baylor, A. Geraud, W. A. Houlberg, D. Frigione, M. Gadeberg, T. C. Jernigan, J. De Kloe, P. Kupschus, B. V. Kuteev, P. Lang, A. A. M. Oomens, A. L. Qualls, K. N. Sato, G. L. Schmidt, Nucl. Fusion 37 (1997) 445

[25] P. T. Lang, G. D. Conway, T. Eich, L. Fattorini, O. Gruber, S. Gunter, L. D. Horton, S. Kalvin, A. Kallenbach, M. Kaufmann, G. Kocsis, A. Lorenz, M. E. Manso, M. Maraschek, V. Mertens, J. Neuhauser, I. Nunes, W. Schneider, W. Suttrop, H. Urano, the ASDEX Upgrade Team, Nucl. Fusion 44 (2004) 665

[26] P. T. Lang, K. Lackner, M. Maraschek, B. Alper, E. Belonohy, K. Gal, J. Hobirk, A. Kallenbach, S. Kalvin, G. Kocsis, C. P. Perez von Thun, W. Suttrop, T. Szepesi, R. Wenninger, H. Zohm, the ASDEX Upgrade Team, JET-EFDA contributors, Nucl. Fusion 48 (2008) 095007